Supersymmetry at the LHC

Bhaskar Dutta[1] [a]

Department of Physics, Texas A&M University, College Station, TX 77843-4242, USA

Abstract. The succes of supersymmetry is beyond any doubt. With the availabilility of the precise measurement of the dark matter content of the universe, SUSY models are used as cosmological connection to particle physics. We are now ready to verify this theory directly at the upcoming large hadron collider (LHC) which is about to start. In this talk I will summarize various search strategies which will be important to measure supersymmetry parameters and establish the cosmological connection.

1 Introduction

We are about to enter an era of major discovery. The trouble-ridden Standard Model (SM) of particle physics needs a major rescue act. The supersymmetric extension of SM (MSSM) seems to have all the important virtues. The Higgs divergence problem is resolved, grand unification of the gauge couplings can be achieved, the electroweak symmetry can be broken radiatively. A dark matter candidate can be obtained in supersymmetric SM. This dark matter candidate can explain the precisely measured 23% of the universe in the WMAP data [1].

We need to have a direct proof of the existence of supersymmetry (SUSY). SUSY particles can be directly observed at the large hadron collider which is about to start. A large range of SUSY parameter space can be investigated. The dark matter allowed regions of SUSY parameter space can be probed and therefore, the connection between cosmology and particle physics can be established on a firm footing. When LHC will be operating, there will be many other experiments e.g. GLAST, PLANCK, XENON100, LUX etc, probing indirectly the SUSY models. It will be very important to have these different experiments to establish the complete picture. The next few years could be the most crucial years to establish the correct theory of nature beyond the SM.

At the LHC, the main production mechanisms for SUSY are $\tilde{q}\tilde{g}$, $\tilde{q}\tilde{q}$, $\tilde{g}\tilde{g}$ etc. Typically, the squarks and gluinos then decay into quarks neutralinos and charginos. The heavier neutralino and charginos then decay into lightest neutralino ($\tilde{\chi}_1^0$ and Higgs, Z, leptons etc. The final state typically has multiple leptons plus multiple jets plus $\not{E}_{\rm T}$. $\tilde{\chi}_1^0$ is the dark matter candidate -since it does not decay into anything. The signal typically has $\sim 10^5$ events per fb^{-1} of luminosity. There will be about $\sim 10^{8-9}$ SM events for the same amount of luminosity which will form the background to our search for SUSY. In order to see the signal beyond the background, the typical event selection is made with large amount of missing energy, high p_T jets, large numbers of jets and leptons.

The SUSY models have new masses and therefore many new parameters. The minimal supersymmetric SM or MSSM has more than hundred parameters. The attempt will be to measure all these parameters at the LHC from the decay chains as described above which is not an easy task. The models based on new symmetries (e.g., grand unification), however, contains less number of parameters and can be probed via the characteristic features of the models. Since these model parameters are also much less than MSSM, one may be able to determine them after measuring a few observables. After we confirm a model from the real data, the next step would be to extract the prediction of the model for cosmology. The parameters of these models will be used to calculate relic density and then we need to compare them with the WMAP results [2]. This is very important since from this exercise, we will also be able to know if there is any need for another dark matter candidate. When the LHC will be operating, these models also will be simultaneously searched at many different experiments, e.g., direct and indirect detection experiments of dark matter, quark and lepton flavor violating decay modes etc.

In this talk, I will concentrate on the specific LHC signals of SUSY models starting from the most simplest one, minimal SUGRA model [3].

2 mSUGRA

The mSUGRA model is a simple model which contains only five parameters:

$$m_0,\ m_{1/2},\ A_0,\ \tan\beta \text{ and } sign(\mu). \qquad (1)$$

m_0 is the universal scalar soft breaking parameter at $M_{\rm GUT}$; $m_{1/2}$ is the universal gaugino mass at $M_{\rm GUT}$;

[a] *Email:* dutta@physics.tamu.edu

A_0 is the universal cubic soft breaking mass at $M_{\rm GUT}$; and $\tan\beta = \langle\hat{H}_1\rangle/\langle\hat{H}_2\rangle$ at the electroweak scale, where $\hat{H}_1$ ($\hat{H}_2$) gives rise to up-type (down-type) quark masses. The model parameters are already significantly constrained by different experimental results. Most important for limiting the parameter space are: (i) the light Higgs mass bound of $M_{h^0} > 114$ GeV from LEP [4], (ii) the $b \to s\gamma$ branching ratio bound of $1.8 \times 10^{-4} < \mathcal{B}(B \to X_s\gamma) < 4.5 \times 10^{-4}$ (we assume here a relatively broad range, since there are theoretical errors in extracting the branching ratio from the data) [5], (iii) the 2σ bound on the dark matter relic density: $0.095 < \Omega_{\rm CDM}h^2 < 0.129$ [1], (iv) the bound on the lightest chargino mass of $M_{\tilde{\chi}_1^\pm} > 104$ GeV from LEP [6] and (v) the muon magnetic moment anomaly a_μ, where one gets a 3.3σ deviation from the SM from the experimental result [7–9]. Assuming the future data confirms the a_μ anomaly, the combined effects of $g_\mu - 2$ and $M_{\tilde{\chi}_1^\pm} > 104$ GeV then only allows $\mu > 0$. The allowed mSUGRA parameter space, at present, has four distinct regions [10]: (i) the stau neutralino ($\tilde{\tau}_1$-$\tilde{\chi}_1^0$) coannihilation region where $\tilde{\chi}_1^0$ is the lightest SUSY particle (LSP)(In fig. 1, this dark matter allowed region is the narrow corridor along $m_{1/2}$ for smaller values of m_0), (ii) the $\tilde{\chi}_1^0$ having a larger Higgsino component (focus point) (In fig. 1, this dark matter allowed region appears for larger values of m_0), (iii) the scalar Higgs (A^0, H^0) annihilation funnel ($2M_{\tilde{\chi}_1^0} \simeq M_{A^0,H^0}$) (For the parameter space of the fig.1, this region appears for larger values of $m_{1/2}$ which is not shown in the figure), (iv) a bulk region where none of these above properties is observed, but this region is now very small due to the existence of other experimental bounds (In fig.1 this region is eclipsed by the bound from $b \to s\gamma$). These four regions have been selected out by the CDM constraint. The allowed parameter space for $\tan\beta$ =40 is shown in fig. 1.

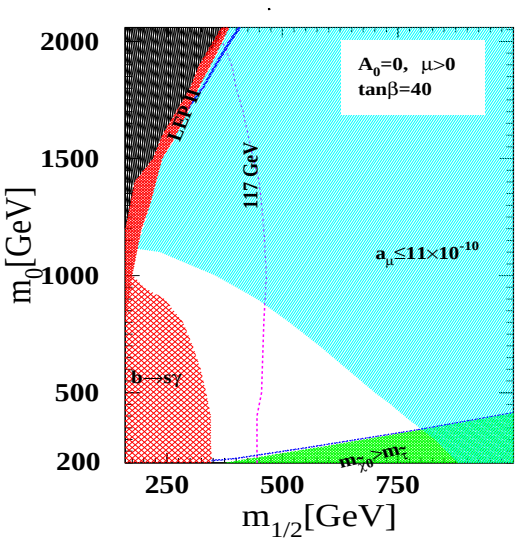

Fig. 1. The narrow ΔM coannihilation band is plotted as a function of $m_{1/2}$ for $\tan\beta = 40$ with $A_0 = 0$ and $\mu > 0$. The left end of the band is due to the $b \to s\gamma$ branching ratio bound and the right end by $a_\mu < 11 \times 10^{-10}$.

3 mSUGRA at the LHC

One of the first analysis for mSUGRA at the LHC will involve the measurement of M_{eff} which is the scalar sum of the transverse momenta of the four leading jets and the missing transverse energy:

$$M_{eff} = p_{T,1} + p_{T,2} + p_{T,3} + p_{T,4} + \not{E}_{\rm T}\,. \qquad (2)$$

The requirement for this measurement are the following: (1) At least four jets with $p_{T,1} > 100\,$GeV and $p_{T,2,3,4} > 50\,$GeV, where the jets are numbered in order of decreasing p_T.(2) $M_{eff} > 400\,$GeV, where (3) $\not{E}_{\rm T} > \max(100\,{\rm GeV}, 0.2{\rm M_{eff}})$. In Fig. 2, the distribution of M_{eff} and the background are shown [11]. The peak of the distribution varies linearly with the Min$[m_{\tilde{q}}m_{\tilde{g}}]$ [11,12] for the mSUGRA model and therefore the scale of SUSY can be surmised from this peak measurement

After we establish the existence of SUSY and an overall scale for the SUSY production, we need to measure the masses. The existence of missing energy in the

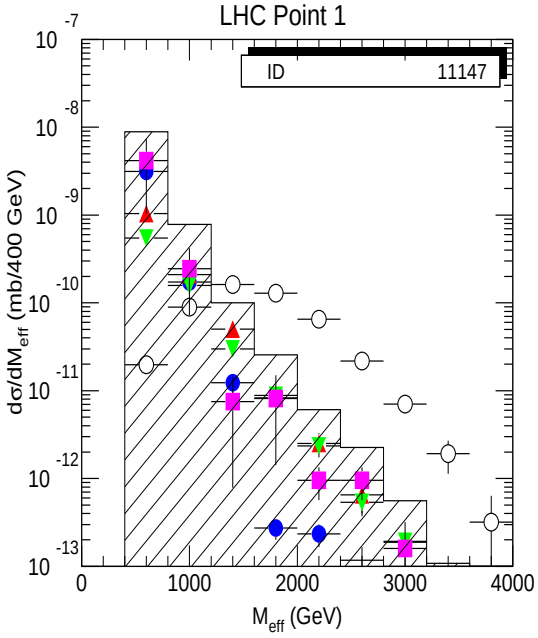

Fig. 2. LHC Point 1 signal and Standard Model backgrounds. Open circles: SUSY signal. Solid circles: $t\bar{t}$. Triangles: $W \to \ell\nu$, $\tau\nu$. Downward triangles: $Z \to \nu\bar{\nu}$, $\tau\tau$. Squares: QCD jets. Histogram: sum of all backgrounds [11]

signal will tell us the possibility of dark matter candidate, but the calculation of the relic density is based on the parameters of the models which depends on the measurement of masses and the mixing matrices.

Now we discuss the mass measurements. Suppose $\tilde{q}_L$ is pair produced and then $\tilde{q}_L$ decays into $\tilde{\chi}_2^0 q$. The

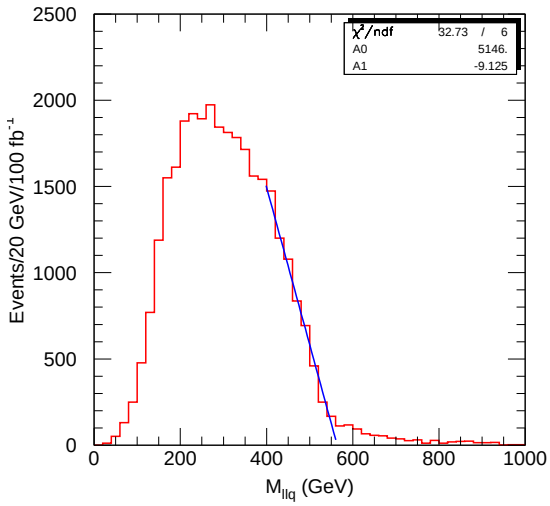

Fig. 3. Mass distribution for the smaller of the two $\ell^+\ell^- q$ masses showing a linear fit near the four-body end point [11].

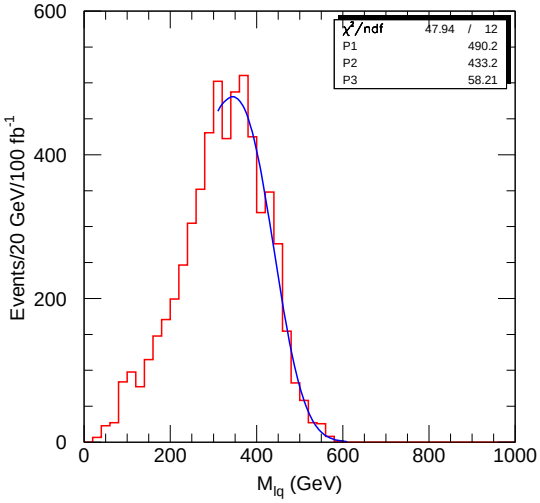

Fig. 4. Distribution of the larger of the two $\ell^{\pm} q$ masses for $\ell^+\ell^- q$ events [11]

$\tilde{\chi}_2^0$ then decays into a pair of opposite sign leptons (via slepton) and $\tilde{\chi}_1^0$. It is expected that the two high energy jets will be arising directly from $\tilde{q}_L \to \tilde{\chi}_2^0 q$ as a dominant production process is that which leads to $\tilde{q}_L \tilde{g}$ and hence to pairs of $\tilde{q}_L$. Therefore, the smaller of the two masses formed by combining the leptons with one of the two highest p_T jets should be less than the four-body kinematic end point for squark decay, e.g.,

$$M_{\ell\ell q}^{\max} = \left[\frac{\left(M_{\tilde{q}_L}^2 - M_{\tilde{\chi}_2^0}^2\right)\left(M_{\tilde{\chi}_2^0}^2 - M_{\tilde{\chi}_1^0}^2\right)}{M_{\tilde{\chi}_2^0}^2} \right]^{1/2} . \quad (3)$$

The distribution of the smaller $\ell^+\ell^- q$ mass is shown in Fig. 3 subtracting the opposite flavor combination

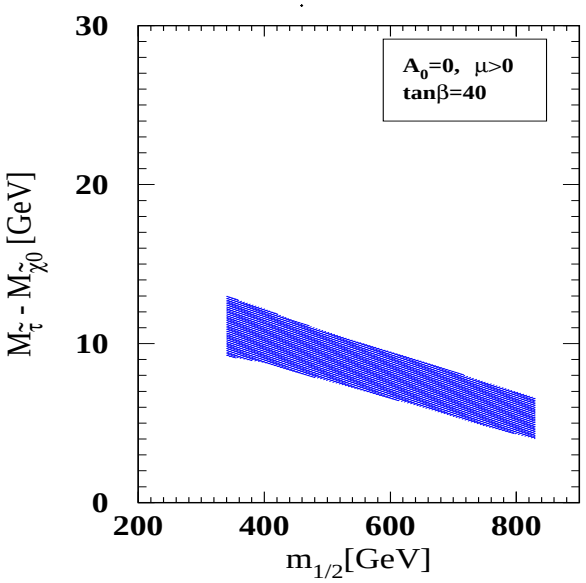

Fig. 5. The narrow ΔM coannihilation band is plotted as a function of $m_{1/2}$ for $\tan\beta = 40$ with $A_0 = 0$ and $\mu > 0$. The left end of the band is due to the $b \to s\gamma$ branching ratio bound and the right end by $a_\mu < 11 \times 10^{-10}$ [13].

from the same flavor lepton pairs. The $e^+e^- + \mu^+\mu^- - e^{\pm}\mu^{\mp}$ combination cancels all contributions from two independent decays and reduces the combinatorial background. Fig. 4 shows a linear fit near the end point for the distribution of the larger of the two $\ell^{\pm} q$ masses for $\ell^+\ell^- q$ events. The end points of $\ell^+\ell^-$, $higgs + q$, $Z + q$ distributions are also used. These types of measurements can be used to determine the masses of the SUSY particles without any choice of model by solving the algebraic equations. These measurement methods to determine the parameters of different mSUGRA allowed parameter space.

4 Stau-Neutralinno Coannihilation

In this region the stau and the neutralino masses are close. The relic density is satisfied by having both stau and neutralino mass to be close and thereby increasing the neutralino annihilation cross section. This phenomenon occurs for a large region of mSUGRA parameter space for smaller values of m_0.

The crucial aspect of the signal is the low energy tau and in the analysis. Fig. 5 shows the range of allowed ΔM values in the coannihilation region as a function of $m_{1/2}$ for $\tan\beta = 40$. We see that ΔM is narrowly constrained and varies from 5-15 GeV. Because of the small ΔM value, τ's from $\tilde{\tau}_1 \to \tau \tilde{\chi}_1^0$ decays are expected to have low energy providing the characteristic feature of the coannihilation region.

We are mostly interested in events from $\tilde{\chi}_1^0 \tilde{\chi}_2^0$, $\tilde{\chi}_1^{\pm} \tilde{\chi}_2^0$, or $\tilde{\chi}_2^0 \tilde{\chi}_2^0$ pairs, where the $\tilde{\chi}_1^0$ in the first case is directly from the $\tilde{q}_R$ decay. The branching ratio of $\tilde{\chi}_2^0 \to \tau\ \tilde{\tau}_1$ is about 97% for our parameter space and is dominant even for large $m_{1/2}$ in the entire coannihilation region;

the same is true for the $\tilde{\chi}_1^{\pm} \rightarrow \nu\ \tilde{\tau}_1$ decay mode. (It should be noted that both $\tilde{e}_R$ and $\tilde{\mu}_R$ are lighter than $\tilde{\chi}_2^0$ by about 10 GeV . However, the branching ratio for $\tilde{\chi}_2^0 \rightarrow e\tilde{e}_R$ or $\mu\tilde{\mu}_R$ is much less than 1%.) Since the stau decays via $\tilde{\tau}_1 \rightarrow \tau\tilde{\chi}_1^0$, we expect inclusive $\tilde{\chi}_2^0$ events to include at least two τ leptons plus large $E_{\rm T}$ jet(s) and large $\not\!\!E_{\rm T}$ (from the $\tilde{\chi}_1^0$).

Two experimental scenarios have been considered [13,14]. The first one uses the $\not\!\!E_{\rm T}$ + $\geq$2 jet final state to reduce backgrounds and searches for the 2τ's that arises from the decays of $\tilde{\chi}_2^0$. In each candidate event, all di-tau pairs can then be searched for a mass peak as evidence of the $\tilde{\chi}_2^0$ decay chain. The second option studies gaugino pairs ($\tilde{\chi}_2^0\tilde{\chi}_2^0$, $\tilde{\chi}_1^{\pm}\tilde{\chi}_2^0$) and requires 3$\tau$'s to reduce backgrounds and only 1 jet + $\not\!\!E_{\rm T}$ in the final state to regain acceptance. Both final states will be triggered by requiring large $E_{\rm T}$ jet(s) and large $\not\!\!E_{\rm T}$ and such a trigger will be available at both the ATLAS and the CMS experiments.

We first examine the visible $p_{\rm T}$ ($p_{\rm T}^{\rm vis}$) distribution of $\tau_{\rm h}$'s from $\tilde{\tau}_1 \rightarrow \tau\tilde{\chi}_1^0$ in $\tilde{\chi}_2^0$ decays with ΔM = 5, 10, and 20 GeV using isajet [15]. As seen in Fig. 6, even with a small mass difference, the τ is boosted in the cascade decay of the heavy squark and gluino making it potentially viable. One can already begin to see the importance of reconstructing the τ's with $p_{\rm T}^{\rm vis} \gtrsim 20$ GeV.

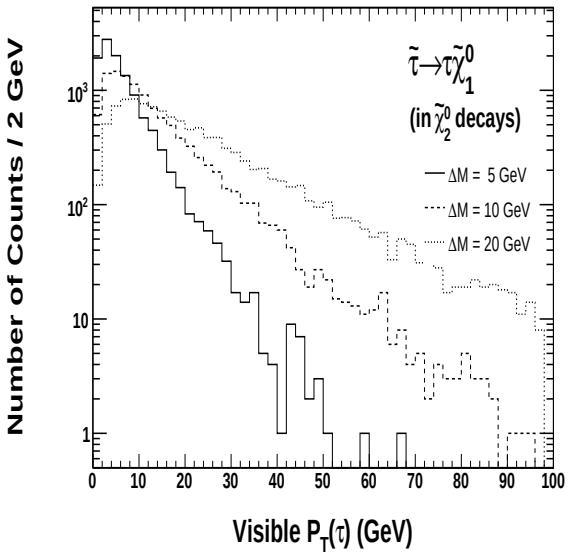

Fig. 6. The visible $p_{\rm T}$ distributions for hadronically decaying τ leptons from $\tilde{\tau}_1 \rightarrow \tau\tilde{\chi}_1^0$ where the $\tilde{\tau}_1$'s are required to be decays of $\tilde{\chi}_2^0 \rightarrow \tau\tilde{\tau}_1$. The curves show the results for ΔM = 5, 10, and 20 GeV.

.

To generate our signal and backgrounds we simulate our model with all SUSY production using ISAJET [15]. We run the generated particles through a detector simulator, PGS [16], using the CDF parameter file for jet finding, and directly use the visible particle 4-momenta for the tau-jet and electron/muon objects.

Table 1. Final selection criteria.

3 identified τ candidates with $\|\eta\| < 2.5$ and $E_T > 40$, 40 and 20 GeV respectively
1 jet with $E_T > 100$ GeV and $\|\eta\| < 2.5$
$\not\!\!E_{\rm T} > 100$ GeV
$\not\!\!E_{\rm T}$+ $E_T^{\rm jet\ 1} > 400$ GeV
$M_{\tau\tau}^{\rm vis} < 100$ GeV where only $\tau_1\tau_3$ and $\tau_2\tau_3$ invariant mass combinations are considered

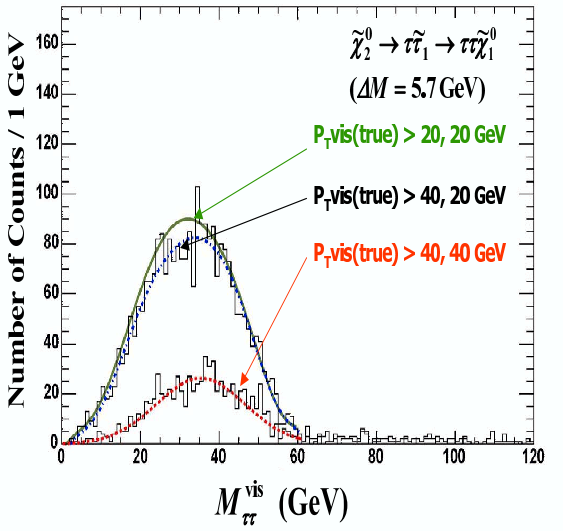

Fig. 7. Using A randomly-selected SUSY sample. A clear peak is visible for $E_T > 40$, 20 GeV and 20, 20 GeV cases in a generator level study.

Finally, a separate Monte Carlo routine assigns the efficiency for τ's and fake rate for jets.

The invariant mass of the τ pair from the $\tilde{\chi}_2^0$ decay forms a distinct mass distribution and provides excellent rejection against both SUSY and SM backgrounds. This can be seen by considering the τ pair in the chain $\tilde{\chi}_2^0 \rightarrow \tau\tilde{\tau} \rightarrow \tau\tau\tilde{\chi}_1^0$ in the rest frame of the $\tilde{\chi}_2^0$. The endpoint is not visible because of the lost neutrinos, but shows a clear peak that still depends mostly on $M_{\tilde{\chi}_2^0}$, $M_{\tilde{\tau}}$, and $M_{\tilde{\chi}_1^0}$.

For each candidate tau pair, $M_{\tau\tau}^{\rm vis}$ is calculated for every pair of τ's in the event and categorized as opposite sign (OS) or like sign (LS). The mass distribution for LS pairs is subtracted from the distribution for OS pairs to extract $\tilde{\chi}_2^0$ decays on a statistical basis. We assume the identification (ID) efficiency (ϵ) to be 100%. Fig. 7 shows the $M_{\tau\tau}^{\rm vis}$ distributions for OS, LS, and OS$-$LS pairs for a hypothetical SUSY sample.

We consider the 3τ's + 1 jet + $\not\!\!E_{\rm T}$ in the final state scenario. (We proceed in the same way if we use the first option). We define our observables, the number of counts, $N_{\rm OS-LS}$, and the visible ditau mass peak position, $M_{\tau\tau}^{\rm peak}$, and describe their values as a function of both ΔM and $M_{\tilde{g}}$. We then show how these two variables can be used to simultaneously measure both ΔM and $M_{\tilde{g}}$.

The variable N_{OS-LS} is the number of LS τ pairs subtracted from the number of OS τ pairs passing all the selection requirements in Table 1. Because we expect the τ_3 to come from the $\tilde{\tau}\rightarrow\tau\widetilde{\chi}_1^0$ decay, the average E_T of the τ_3 (its probability of having $E_T^{\tau_3} > 20$ GeV), and therefore, N_{OS-LS} grows with ΔM. Thus, for a known luminosity, a measurement of N_{OS-LS} allows for a determination of ΔM. An increase in $M_{\tilde{g}}$ affects N_{OS-LS} by decreasing the production rate of gluinos, which decreases the number of $\widetilde{\chi}_2^0$ decay chains produced. Though mass changes in squarks and other gauginos also modify both production and boost, the mSUGRA relations relate these directly to ΔM and $M_{\tilde{g}}$. We can write

$$N_{OS-LS} \propto \sigma(M_{\tilde{g}}) \cdot A(\Delta M, M_{\tilde{g}}), \qquad (4)$$

where σ is the total production cross section, A is the acceptance, and $M_{\tilde{g}}$ effectively provides a scale for the model. Figs. 8 and 9 show N_{OS-LS} as a function of ΔM and $M_{\tilde{g}}$. We see that N_{OS-LS} is flat below ΔM ~5 GeV and nearly linear above it as a function of ΔM. At low ΔM, the number of τ pairs from single $\widetilde{\chi}_2^0$ decays goes to zero as none of the τ's from $\tilde{\tau}$ decay pass the 20 GeV threshold; however, N_{OS-LS} does not go to zero because of the small SUSY background from stop quark pair production and decay via $\widetilde{t}_1\rightarrow t\widetilde{\chi}_i^0\rightarrow(Wb)\widetilde{\chi}_i^0\rightarrow(\tau\nu)b\widetilde{\chi}_i^0$. This background is independent of ΔM, so the small number of events in the very low ΔM region implies that it is negligible. As expected N_{OS-LS} falls steeply as a function of $M_{\tilde{g}}$

We define $M_{\tau\tau}^{\rm peak}$ as the position of the peak of the visible ditau invariant mass distribution after the LS distribution is subtracted from the OS distribution. It directly depends on ΔM. $M_{\tau\tau}^{\rm peak}$ rises as a function of ΔM (shown in Fig. 10). As $M_{\tilde{g}}$ changes, so do $M_{\widetilde{\chi}_2^0}$ and $M_{\widetilde{\chi}_1^0}$, which leads to $M_{\tau\tau}^{\rm peak}$ rising as a function of $M_{\tilde{g}}$; this result is shown in Fig. 11.

Fig. 12 shows the expected uncertainty on ΔM as a function of ΔM and the expected percent uncertainty on ΔM and $M_{\tilde{g}}$ as functions of luminosity for $\Delta M = 9$ GeV and $M_{\tilde{g}} = 850$ GeV. Note that we have used the 1σ intersecting lines as they conservatively overestimate our systematic error. We find that for $\mathcal{L}$ = 30 fb^{-1} we can measure ΔM to ~15% and $M_{\tilde{g}}$ to ~6%. For 10 fb^{-1}, these uncertainties become 20% and 9% respectively.

It is possible to use some more observables. One can use the p_T distribution of the low energy tau. This is a very important observable since the measurement of a low energy tau in the signal will be a smoking gun signal for the coannihilation. The peak positions of the $M_{j\tau\tau}$ (shown in Fig. 13) and $M_{j\tau}$ distributions are also very useful observable. Combining all these observables one can measure the following masses: $\tilde{q}_L$, $\tilde{g}$, $\tilde{\chi}_2^0$, $\tilde{\chi}_1^0$, $M_{\tilde{\tau}_1}$. One can use these masses to solve for the mSUGRA parameters m_0, $m_{1/2}$ for fixed $\tan\beta$ and A_0 values (shown in Fig. 14). The accuracy of the determination are about 2% for m_0 and $m_{1/2}$ for 10 fb^{-1} of luminosity. Now combining all these measurements one can determine the accuracy of Ωh^2 for a fixed A_0 and $\tan\beta$. In Fig. 15, we show that the relic density can be measured with an accuracy of 5-6%.In order to complete the mSUGRA model determination, one needs to determine $\tan\beta$ and A_0 which involves the stop and sbottom sector. The individual measurements of the stop and sbottom masses can be hard but it may be possible to measure the parameters A_0 and $\tan\beta$ [17].

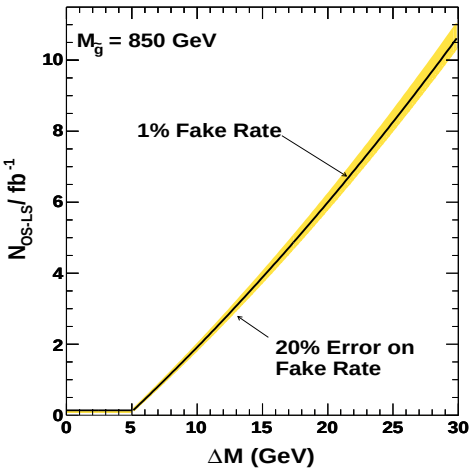

Fig. 8. We show N_{OS-LS} as a function of ΔM with a 1% fake rate with the shaded band representing the variation due to the 20% systematic uncertainty on the $\tau \rightarrow$ jet fake rate. Below ~5 GeV, the third τ from $\tilde{\tau}\rightarrow\tau\widetilde{\chi}_1^0$ is so soft that there is no signal; therefore, counting is dominated by SUSY backgrounds, and the number of counts is flat. Above ~5 GeV, the number of counts is nearly linear as a function of ΔM as more and more τ's from $\tilde{\tau}\rightarrow\tau\widetilde{\chi}_1^0$ pass the 20 GeV threshold [14].

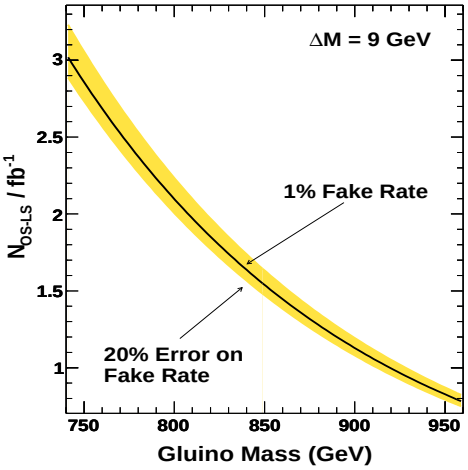

Fig. 9. This plot shows the relationship between N_{OS-LS} and $M_{\tilde{g}}$ for $\Delta M = 9$ GeV; N_{OS-LS} decreases strongly with increasing $M_{\tilde{g}}$ as larger masses drive down the total production cross section [14].

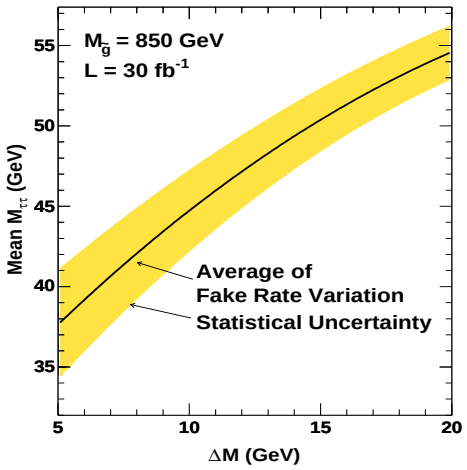

Fig. 10. The $M_{\tau\tau}^{\text{peak}}$ increases strongly with both increasing ΔM [14].

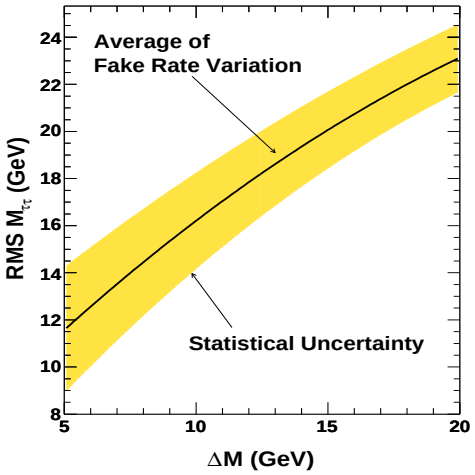

Fig. 11. The $M_{\tau\tau}^{\text{peak}}$ increases strongly with both increasing $M_{\tilde{g}}$ [14]

.

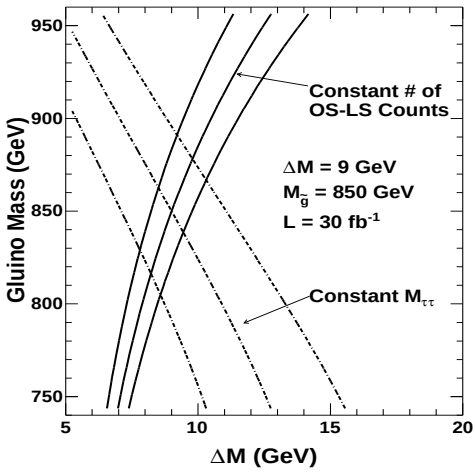

Fig. 12. The contours of constant N_{OS-LS} and $M_{\tau\tau}^{\text{peak}}$ for ΔM = 9 GeV, $M_{\tilde{g}}$ = 850 GeV, and $\mathcal{L}$ = 30 fb^{-1}. The middle lines are the central values while the outer lines show the 1σ uncertainty on the measurements. The region defined by the outer four lines indicates the 1σ region for the ΔM and $M_{\tilde{g}}$ measurements [14].

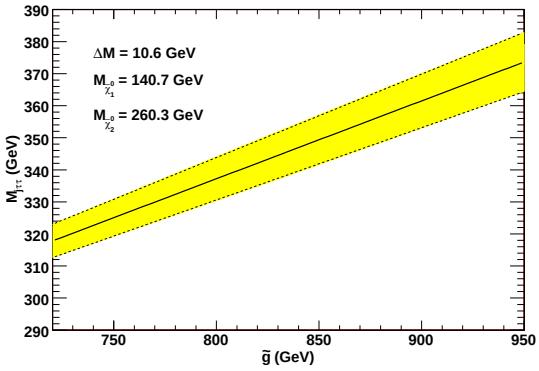

Fig. 13. $M_{j\tau\tau}^{\text{peak}}$ vs. gluino mass

5 Focus point

In this region, m_0 is very large, but $m_{1/2}$ can be small which means the gaugino masses can be small. For a fixed value of the parameter $m_{1/2}$ in the mSUGRA model, if m_0 is taken to be of order the weak scale, then $m_{H_u}^2$ is driven to negative values at the weak scale due to the large top quark Yukawa coupling in the RGEs, whereas if m_0 is taken too large, then the GUT scale value of $m_{H_u}^2$ is so high that it does not become negative values when the weak scale is reached in RG running. Intermediate to these two extreme cases there exists a region where μ^2 is found to be zero, which forms the large m_0 edge of parameter space. If μ^2 is positive, but tiny, then light higgsino-like charginos will be generated and one needs to be worried about the LEP limit on chargino masses which require $m_{\tilde{\chi}_1^\pm} > 103.5$ GeV. If μ^2 is large enough to evade LEP2 limits, then large higgsino-bino mixing occurs in the chargino and neutralino sectors, the lightest neutralino becomes a mixed higgsino-bino dark matter particle. A lightest neutralino of mixed higgsino-bino form has a large annihilation rate, and hence satisfy the WMAP measurements. In the WMAP-allowed focus point region, since squarks have masses in the TeV range, only three-body decay modes of the gluino are allowed. The third generation quark-squark-neutralino/chargino couplings are enhanced by top quark Yukawa coupling terms since the neutralino and chargino can have large higgsino component.

One search strategy of this region is to study the shape of dilepton final state. The dileptons are produced from $\tilde{\chi}_3^0$ and $\tilde{\chi}_2^0$ decays. Using the parameter space, m_0=3550 GeV; $m_{1/2}$=300 GeV; A_0=0; tan β=10 ; μ >0, Tovey etal has shown that the gaguino mass differences can be measured with an accuracy of 1 GeV. This error can be improved up to 0.5 GeV [19].

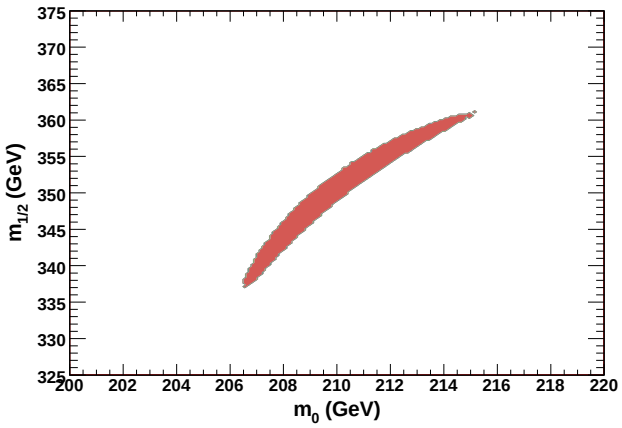

Fig. 14. Error Ellipse plotting the uncertainty on m_0 vs $m_{1/2}$.

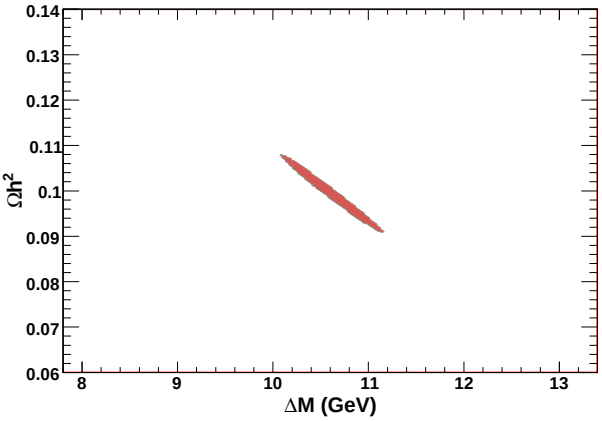

Fig. 15. Error Ellipse plotting the uncertainty on Ωh^2 vs ΔM.

In the reference [20], it is shown that by requiring high jet and b-jet multiplicity, and a high effective mass cut, a rather pure signal arises over the dominantly $t\bar{t}$ SM background. Since the signal came almost entirely from gluino pair production, and the decay branching fractions were fixed by assuming the neutralino relic density saturated the WMAP $\Omega_{\tilde{\chi}_1^0}h^2$ measurement, the total signal rate has been used to extract an estimate of the gluino mass. It is found in the reference [20] that, $m_{\tilde{g}}$ could be measured to a precision of about 8% for 100 fb^{-1} of integrated luminosity. In order to make this measurement, the signal contains $n \geq 7$ jets, $n \geq 2$ b-jets and $A_T = E_T(miss) + \Sigma E_T(jet) + \Sigma E_T(lepton > 1300$ GeV with $100 fb^{-1}$ luminosity. The A_T distribution in events with ≥ 7 jets and ≥ 2 b-tags, for the model point $m_0 = 3050$ GeV, $m_{1/2} = 400$ GeV, $A_0 = 0$,tan $\beta = 30$, $\mu > 0$ is shown in figure 16.

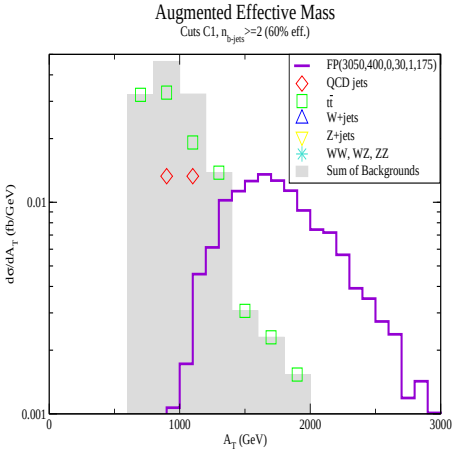

Fig. 16. Distribution of A_T in events with ≥ 7 jets and ≥ 2 b-tags, for the model point $m_0 = 3050$ GeV, $m_{1/2} = 400$ GeV, $A_0 = 0$,tan $\beta = 30$, $\mu > 0$ and $m_t = 175$ GeV, versus various SM backgrounds [20].

In addition, the signal from this region can be separated as to its isolated lepton content. The OS/SF dilepton mass distribution embedded in the hard signal component should exhibit mass edges at $m_{\tilde{\chi}_2^0} - m_{\tilde{\chi}_1^0}$ and also at $m_{\tilde{\chi}_3^0} - m_{\tilde{\chi}_1^0}$, which are distinctive of this scenario in which the LSP is a mixed bino-higgsino particle. The mass-difference edges, along with the absolute gluino mass, may provide enough information to constrain the absolute chargino and neutralino masses.

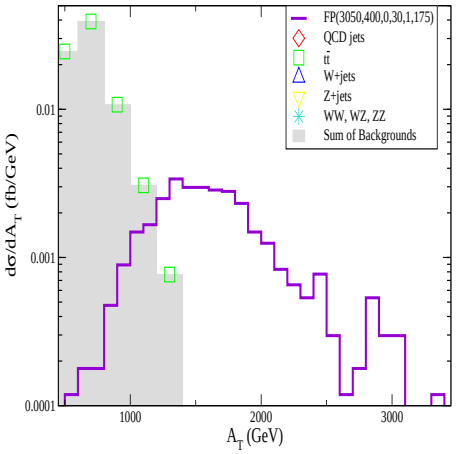

Fig. 17. Distribution in A_T of events with cuts C1, $n(leps) \geq 2$, $n(b-jets) \geq 2$ and $n(jets) \geq 4$ for the same parameter space point as above[20].

Large m_0 region also explains the EGRET excess of diffuse galactic gamma rays by supersymmetric dark matter annihilation. The SUSY parameter space for this region: m_0=1400 GeV, tan β=50 $m_{1/2}$=180 GeV, A_0=0.5 m_0 [21].

6 Bulk Region

In this region, the relic density constraint is satisfied by t channel selectron, stau and sneutrino exchange. Nojiri et al [22] has analyzed the bulk region by measuring the masses from the end point measurements. The parameter pace point is m_0=70 GeV; $m_{1/2}$=250 GeV; A_0=-300; $\tan\beta$=10 ; μ >0 for the analysis of the bulk region. The end points have been determined for the lq, llq, ll etc distributions as described before and are given in Table 2.

Table 2. Table of the SUSY measurements which can be performed at the LHC with the ATLAS detector [22]. The central values are calculated with ISASUSY 7.71, using the tree-level values for the sparticle masses. The statistical errors are given for the integrated luminosity of 300 fb^{-1}. The uncertainty in the energy scale is taken to result in an error of 0.5% for measurements including jets, and of 0.1% for purely leptonic mesurements [22].

Variable	Value (GeV)	Error
$m_{\ell\ell}^{max}$	81.2	0.09
$m_{\ell\ell q}^{max}$	425.3	2.5
$m_{\ell q}^{low}$	266.9	1.6
$m_{\ell q}^{high}$	365.9	2.1
$m_{\ell\ell q}^{min}$	207.0	1.9
$m(\ell_L) - m(\tilde{\chi}_1^0)$	92.3	1.6
$m_{\ell\ell}^{max}(\tilde{\chi}_4^0)$	315.8	2.3
$m_{\tau\tau}^{max}$	62.2	5.0

The measurement of the sparticle masses are done from the measured edges. The error is of ∼9 GeV for the masses of the sparticles. The distribution of the measured $\tilde{\chi}_1^0$ masses for a set of Monte Carlo experiments is shown in Fig. 18. Since the masses are determined from a set of algebraic equations the errors are strongly correlated. The mass difference is strongly constrained (e.g., $m(\tilde{l}_R) - m(\tilde{\chi}_1^0)$ is ∼ 200 MeV due to the very good precision of the edge measurements, but the absolute error has loose constrained sim ∼ 9 GeV. The calculated precision on $m(\tilde{\tau}_1) - m(\tilde{\chi}_1^0)$ is ∼ 2.5 GeV. In this case the stau neutralino mass difference is larger than the neutralino-stau coannihilation region. The τs are more energetic in this case. After putting all the measurements together, the relic density is calculated in this scenario with an accuracy 0.1080.01(stat + sys) with a luminosity of 200 fb^{-1}.

7 Other Models

We first discuss a very important extension of the mSUGRA model:

Higgs nonuniversality In these types of models, the Higgs masses are nonuniversal at the GUT scale, $m_{H_1}^2 = m_0^2(1+\delta_1)$ and $m_{H_2}^2 = m_0^2(1+\delta_2)$, where the δ_is are nonuniversal parameters. The constraints on the parameter space of these scenarios are discussed in

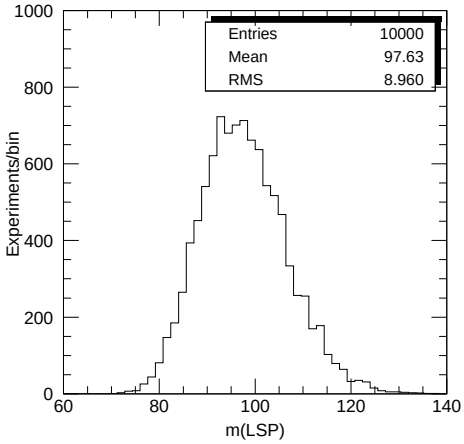

Fig. 18. *Distribution of the measured value of $m(\tilde{\chi}_1^0)$ for a set of Monte Carlo experiments, each corresponding to an integrated statistics of 300 fb^{-1}. The $m(\tilde{\chi}_1^0)$ mass in the model is 97.2 GeV [22].*

the references [23,24]. There can be two different types of Higgs non universality: case (1) $m_{H_u}^2 = m_{H_d}^2 \neq m_0^2$ at M_{GUT}. In this case, the parameter space of this one parameter extension of the mSUGRA model is given by,

$$NUHM1 : m_0,\ m_\phi,\ m_{1/2},\ A_0,\ \tan\beta \text{ and } sign(\mu). \quad (5)$$

The second case is inspired by GUT models where H_u and H_d belong to different multiplets and $m_{H_u}^2 \neq m_{H_d}^2$ at M_{GUT}. The parameter space for this second case is then given by

$$NUHM2 : m_0,\ m_{H_u}^2,\ m_{H_d}^2,\ m_{1/2},\ A_0,\ \tan\beta \text{ and } sign(\mu). \quad (6)$$

The first case can have two regions of dark matter allowed: Higgsino region and A funnel. In the Higgsino region of the NUHM1 model, charginos and neutralinos are light, and more easily accessible to collider searches. In addition, lengthy gluino and squark cascade decays to the various charginos and neutralinos occur, leading to the possibility of spectacular events at the LHC. In the A-funnel region, the A, H and $H^\pm$ Higgs bosons are lighter and appear in the final stages of cascades at the CERN LHC. In the second case, since μ and m_A can now be used as input parameters, it is always possible to choose values such that one lies either in the higgsino annihilation region or in the A-funnel region, for any value of $\tan\beta$, m_0 or $m_{1/2}$ that gives rise to a calculable SUSY mass spectrum. In the low μ region, charginos and neutralinos are again likely to be light, and accessible to to the LHC searches. If instead one is in the A-annihilation funnel, then the heavier Higgs scalars may be light enough to be produced at observable rates. In addition, new regions are found where consistency with WMAP data is obtained because either $\tilde{u}_R$, $\tilde{c}_R$ squarks or left- sleptons become very light. The $\tilde{u}_R$ and $\tilde{c}_R$ co-annihilation region leads

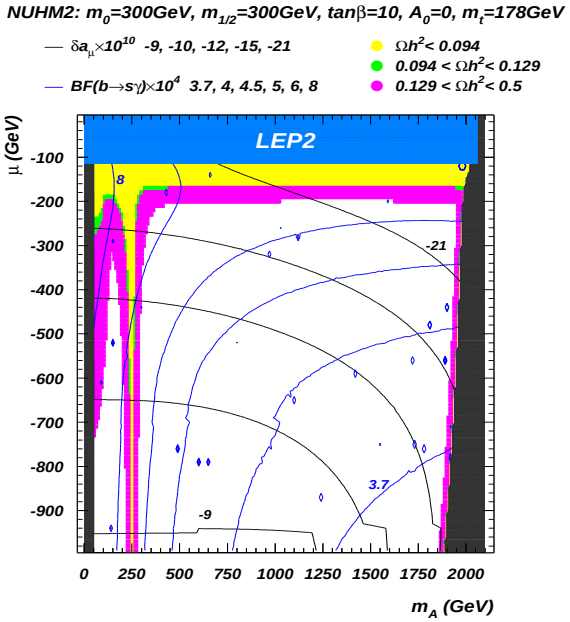

Fig. 19. Ranges of $\Omega_{\tilde{\chi}_1^0}h^2$ together with contours of $BF(b \to s\gamma)$ and Δa_μ in the μ *vs.* m_A plane for $m_0 = m_{1/2} = 300$ GeV, $A_0 = 0$, $\tan\beta = 10$ and $m_t = 178$ GeV for $\mu > 0$. For very large values of m_A, the stau coannihilation region arises [24].

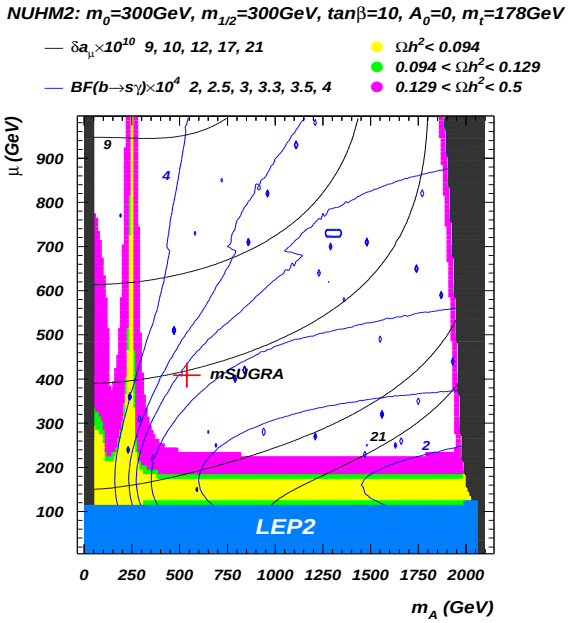

Fig. 20. Same as in previous Fig. 19 for $\mu < 0$ case [24].

to large rates for direct and indirect detection of neutralino dark matter. In both models the A annihilation funnel can occur for ant $\tan\beta$. In Figs. 19 and 20, the ranges of $\Omega_{\tilde{\chi}_1^0}h^2$ together with contours of $BF(b \to s\gamma)$ and Δa_μ in the μ *vs.* m_A plane for $m_0 = m_{1/2} = 300$ GeV is shown for the NUHM2 model.

There exist many more very interesting dark matter allowed SUSY models. I am just mentioning a few of them below. In KKLT type moduli mediation [25], the soft masses have been calculated. The ratio of anomaly mediation and modular mediation is given by a phenomenological parameter α. The mass spectrum is different from the mSUGRA models since the unification of the scalar masses happen at a scale smaller than the GUT scale. Similar situation also arise in GUT less model [26]. In these models, the scale of SUSY breaking soft masses has been assumed to be smaller than the GUT scale.

The nonminimal models (with an additional singlet) also possess interesting signatures and phenomenologies. These models can have smaller lightest Higgs mass and this Higgs can decay into a pair of psedoscalar Higgs [27].

In Compressed MSSM, the gluino mass is small in order to have smaller μ [28]. These models have many top quarks in the final states at the LHC.

The flat directions LLe and udd within the minimal supersymmetric Standard Model provide all the necessary ingredients for a successful inflation with the right amplitude of the scalar density perturbations, negligible gravity waves and the spectral tilt within 2σ observed range $0.92 \leq n_s \leq 1.0$ [29]. Remarkably for the inflaton, which is a combination of squarks and sleptons, there is a stau-neutralino coannihilation region below the inflaton mass 500 GeV for the observed density perturbations and the tilt of the spectrum.

There also exists models where right sneutrino is a successful dark matter candidate [30]. Inflation can be explained in such models in terms of flat directions which involves the interaction terms involving neutrinos [31]. These models have spin zero dark matter. The signal of this model is similar to what we observe in the regular SUGRA models with neutralino being the dark matter candidate, only difference is however in the fact that this model has a spin zero dark matter. The probing of the spin therefore will lead to the discovery of this model.

8 Conclusion

The cosmological connection of the particle physics models can be established at the the LHC. In order to achieve this the SUSY model parameters need to be measured with a great accuracy. In this talk, I discussed the minimal SUGRA model which is a well motivated minimal model of SUSY. The features of this model which are associated with the dark matter explanation are general, i.e. can show up in other models. In the minimal SUGRA model, the stau neutralino coannihilation region appears for smaller values of sparticle massees. In this region however, there exists low energy taus. It is possible to measure observables with these taus with good accuracy and therefore, the relic density can be measured with good accuracy in this model parameter space. The gaugino masses can be measured with less than 10% accuracy in the focus point region. The bulk region (which is less favored) can also be investigated quite precisely with a very accurate determination of the relic density. There

are many other SUSY models with different characteristic signals. The special features of these models will be investigated at the LHC. One interesting scenario is the right handed sneutrino being the dark matter candidate. In this case, the signal could be the same but the spin of the dark matter particle is different. The measurement of the spin of the missing particle will establish one scenario over the other.

This work was supported in part by the DOE grant DE-FG02-95ER40917. I would like to thank the conference organizer for organizing this great meeting. I would also like to thank my collaborators Richard Arnowitt, Adam Arusano, Rouzbeh Allahverdi, Alfredo Gurrola, Teruki Kamon, Nikolay Kolev, Abram Krislock, Anupam Mazumdar, Yukihiro Mimura and Dave Toback for the works related to this talk.

References

1. WMAP Collaboration, D.N. Spergel *et al.*, Astrophys. J. Suppl. **148**, (2003) 175.
2. B. C. Allanach, G. Belanger, F. Boudjema and A. Pukhov, JHEP **0412**, 020 (2004)
3. D.Z. Freedman, P. Van Niewenhuisen, and S. Ferrara, Phys. Rev. D **13**, (1976) 3214; S. Deser and B. Zumino, Phys. Lett. B **65**, (1976) 369; A.H. Chamseddine, R. Arnowitt, and P. Nath, Phys. Rev. Lett. **49**, (1982) 970; R. Barbieri, S. Ferrara, and C.A. Savoy, Phys. Lett. B **119**, (1982) 343; L. Hall, J. Lykken, and S. Weinberg, Phys. Rev. D **27**, (1983) 2359; P. Nath, R. Arnowitt, and A.H. Chamseddine, Nucl. Phys. B **227**, (1983) 121; For a review, see P. Nilles, Phys. Rep. **100**, (1984) 1.
4. ALEPH, DELPHI, L3, OPAL Collaborations, G. Abbiendi, *et al.*, (The LEP Working Group for Higgs Boson Searches), Phys. Lett. B, **565**, (2003) 61.
5. M. Alam etal, Phys. Rev. Lett. **74**, (1995) 2885.
6. Particle Data Group, S. Eidelman *et al.*, Phys. Lett. B, **592**, (2004) 1.
7. Muon $g-2$ Collaboration, G. Bennett *et al.*, Phys. Rev. Lett. **74**, (2004) 161802.
8. M. Davier, hep-ex/0312065.
9. K. Hagiwara, A. Martin, D. Nomura, and T. Teubner, Phys. Rev. D**69**, (2004) 093003.
10. J. Ellis, K. Olive, Y. Santoso, and V. Spanos, Phys. Lett. B, **565**, (2003) 176; R. Arnowitt, B. Dutta, and B. Hu, hep-ph/0310103; H. Baer, C. Balazs, A. Belyaev, T. Krupovnickas, and X. Tata, JHEP**0306**, (2003) 054; B. Lahanas and D.V. Nanopoulos, Phys. Lett. B, **568**, (2003) 55; U. Chattopadhyay, A. Corsetti, and P. Nath, Phys. Rev. D**68**, (2003) 035005; E. Baltz and P. Gondolo, JHEP **0410** (2004) 052; A. Djouadi, M. Drees and J. L. Kneur, JHEP **0603**, (2006) 033; J. L. Feng, K. T. Matchev and F. Wilczek, Phys. Lett. B **482**, (2000), 388; G. Belanger, S. Kraml and A. Pukhov, Phys. Rev. D **72**, (2005) 015003;
11. I. Hinchlife and F.E. Paige, Phys. Rev. D**61**, (2000) 095011; I. Hinchliffe, F.E. Paige, M.D. Shapiro, J. Soderqvist, and W. Yao, Phys. Rev. D**55**, (1997) 5520.
12. D. R. Tovey, Phys. Lett. B **498**, (2001) 1.
13. R. Arnowitt, B. Dutta, T. Kamon, N. Kolev and D. A. Toback, Phys. Lett. B **639**, (2006) 46.
14. R. Arnowitt *et al.*, Phys. Lett. B **649**, (2007) 73.
15. F. Paige, S. Protopescu, H. Baer, and X. Tata, hep-ph/0312045.
16. PGS is a parameterized detector simulator. We used version 3.2 (see http://www.physics.ucdavis.edu/~conway/research/software/pgs/pgs general.htm).
17. Work in progress.
18. Talk by D. Tovey, talk at PPC 07.
19. Talk by G. Moortgat-Pick at SUSY 07.
20. H. Baer, V. Barger, G. Shaughnessy, H. Summy and L. t. Wang, Phys. Rev. D **75**, (2007) 095010.
21. W. de Boer, C. Sander, V. Zhukov, A. V. Gladyshev and D. I. Kazakov, Phys. Rev. Lett. **95**, (2005) 209001.
22. M. M. Nojiri, G. Polesello and D. R. Tovey, JHEP **0603**, (2006) 063.
23. J. R. Ellis, A. Ferstl, K. A. Olive and Y. Santoso, Phys. Rev. D **67**, 123502 (2003);
24. H. Baer, A. Mustafayev, S. Profumo, A. Belyaev and X. Tata, JHEP **0507**, (2005) 065.
25. S. Kachru, R. Kallosh, A. Linde and S. P. Trivedi, Phys. Rev. D **68**, (2003)046005 (2003); K. Choi, A. Falkowski, H. P. Nilles and M. Olechowski, Nucl. Phys. B **718**, (2005) 113; K. Choi, K. S. Jeong and K. I. Okumura, JHEP **0509**, (2005) 039; A. Falkowski, O. Lebedev and Y. Mambrini, JHEP **0511**, (2005) 034; H. Baer, E. K. Park, X. Tata and T. T. Wang, JHEP **0608**, (2006) 041; JHEP **0706**, 033 (2007).
26. J. R. Ellis, K. A. Olive and P. Sandick, Phys. Lett. B **642**, (2006) 389.
27. for example, R. Dermisek and J. F. Gunion, Phys. Rev. Lett. **95**, (2005) 041801.
28. S. P. Martin, Phys. Rev. D **76**, (2007) 095005; H. Baer, A. Box, E. K. Park and X. Tata, JHEP **0708**, (2007) 060 (2007).
29. R. Allahverdi, B. Dutta and A. Mazumdar, Phys. Rev. D **75**, (2007) 075018.
30. J. McDonald, JCAP **0701**, (2007) 001. C. Arina and N. Fornengo, arXiv:0709.4477. T. Asaka, K. Ishiwata and T. Moroi, Phys. Rev. D **75**, (2007) 065001. H. S. Lee, K. T. Matchev and S. Nasri, Phys. Rev. D **76**, (2007) 041302.
31. R. Allahverdi, B. Dutta and A. Mazumdar, arXiv:0708.3983 [to appear in Phys Rev. Lett].